CHAPTER ONE

INTRODUCTION AND THEORETICAL REVIEW

1.1 Introduction

II-VI compound materials were the earliest materials used on a large scale for the production of semiconductors. In the third decade of this century they became well known as "crystal phosphors" and were used as cathode-ray tube screen materials; they had a boom in color television tubes in the late fifties and their present production output is nearly comparable with Si. Of course their outstanding merits are not in their semi-conducting properties which have to compete with Si but nevertheless they are semiconductors - adequately understandable and describable by the concepts of semiconductor physics [1].

The twelve binary compounds formed by the metals Zn, Cd, and Hg of column II of the periodic table and the chalcogens O, S, Se, and Te of column VI possess relatively wide energy gaps between the valence and conduction bands. The fact that most of these compounds exhibit direct gaps gives them a great advantage, that is higher optical transmission probabilities for absorption and luminescence. It was just this advantage which was used in the early days for luminescence in the visible region. The high ionicity of these compounds makes them good candidates for having high electro-optical coupling and electromechanical coupling constants [1]. In the last 50 years, interest in the physical properties of the II-VI compounds has stimulated considerable research into methods for growing single crystals as well as thin films of these materials [1-3].

ZnS and ZnSe among II-VI compounds have received a great deal of interest in the preparation and characterization for both academic research and industrial purposes [4-39]. Recently, interest in these materials has c nsiderably increased as much attention has been paid to the development and application of various photoelectric devices. ZnS and ZnSe have been found to be very promising candidates for such technological applications, especially for light emitting diodes (LED's) and heterojunction devices [1,18,40]. The fact that ZnS and ZnSe have almost identical crystallographic features (i. e. both have zincblende structure with lattice constant differs only by less than 5%) has encouraged the researchers to prepare ternary alloys of ZnS_xSe_{1-x}. The preparation of ZnS_xSe_{1-x} alloys is of interest, since it was realized [41] that compounds with physical properties in the intermediate range to that of ZnS and ZnSe could be obtained. For example, depending on the amount of sulphur in the alloy, materials with energy gaps between 2.7 and 3.7 eV, within which there is the major part of the solar radiation, can be prepared. This makes Zn-S-Se alloys attractive for use as a wide band gap window in heterojunction photovoltaics [42]. Therefore, efforts have been centered on preparation of ZnS_xSe_{1-x} in order to obtain materials with the desired electronic and optical properties [42-57]. Different methods and techniques of preparation such as hydrogen transport [42, 44, 48], metal-organic vapor-phase epitaxy [45, 47, 50, 55], thermal vacuum evaporation [51], iodine vapor transport [52, 53] and molecular beam epitaxy [56] were used to prepare crystals and thin films of ZnS_xSe_{1-x} materials. However, electron-beam evaporation technique has received the least attention in order to prepare thin films of ZnS_xSe_{1-x}. It is therefore proposed that more attention should be drawn to the electron-beam evaporation as a technique to deposit thin films of ZnS_xSe_{1-x}.

The aim of this work is to employ the electron beam evaporation technique to prepare thin films of ZnS_xSe_{1-x} onto glass substrates and to study the structure, optical and electrical properties of these films as functions of the film composition. The rest of this chapter will discuss the methods of thin film preparation and some theoretical background of the optical and electrical properties of semiconductors thin films generally, and ZnS_xSe_{1-x} specifically.

In **chapter 2** the experimental work and the equipment used in this work will be described.

Chapter 3 will be devoted to the method of calculation that has been used to estimate the thickness and optical parameters of the samples.

The results obtained in this work are divided into three parts, the film structure, optical properties, and electrical characteristics. These results will be presented in **chapters 4**, **5** and **6**, respectively.

And finally, **chapter 7** will conclude the interesting findings gained from this work with some suggestions for further work.

1.2 Methods of thin film preparation

Thin film deposition onto bulk materials (substrates) contains three main sequential steps. A source of film material is provided, the material is transported to the substrate and finally deposition takes place [58]. The source of the film forming the material may be solid, liquid, vapour or gas. The evaporation of the solid source material can be done by physical processes like heating or by an energetic beam of electrons, photons, or ions (sputtering). These methods are categorized as physical vapour deposition (PVD). Thin film processes that use gases, evaporating liquids, or chemically gasified solids as source materials are categorized as chemical vapour deposition (CVD). In the transport step, high vacuum or gaseous fluids can be used as

a transport medium. In a high vacuum, molecules travel from the source to the substrate in straight lines, whereas in a fluid there are many collisions among molecules during the transport step. Consequently, in a high vacuum, uniformity of source material arrival rate at the substrate is determined by geometry, whereas in a fluid it is determined by gas flow patterns and by diffusion of the source molecules through the other gases present. However, a partially ionized gas, which is known as "plasma", is used in many thin film processes as a transport medium. Plasma contains a great deal of energy, which can activate film deposition processes at low temperature. The plasma operating pressure can be such that it behaves either as a fluid or as a high vacuum medium. The deposition of the film onto the substrate surface is determined by source, and transport factors and by conditions of the deposition surface which are substrate surface conditions, reactivity of the arriving material and energy input. These three deposition factors of substrate condition work together with the arriving fluxes to determine the structure and composition of the deposited film and hence, the film properties. Based on these main steps of thin film deposition, a large number of techniques have been developed to obtain thin films by physical or chemical methods of deposition. The details and specification of each method and technique can be found in the literature, which concerns thin film preparation [1, 2, 3, 59-63]. Deposition by electron-beam evaporation will be described below.

Electron-beam evaporation

Figure 1.1 shows a schematic diagram of a typical electron-beam evaporator. In this technique an intense beam of high-energy electrons is used to evaporate the source material. Electrons thermionically emitted from a hot filament and accelerated into the source material can generate enough energy density to evaporate any material

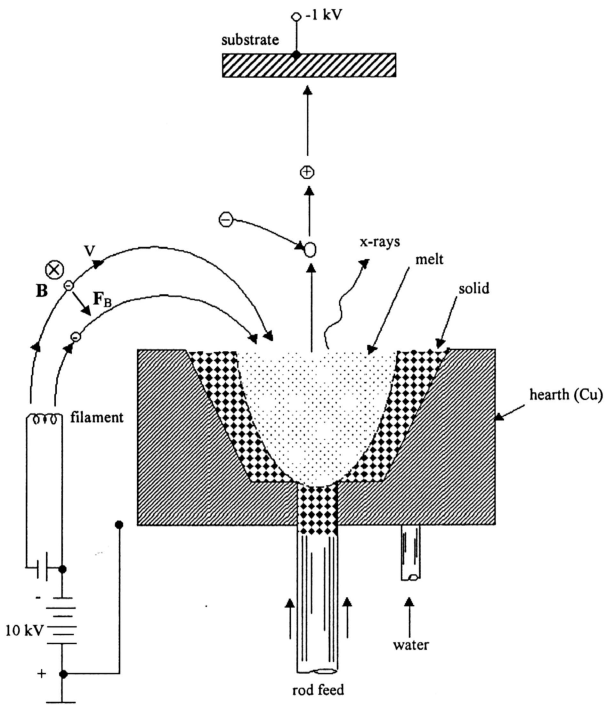

Figure 1.1: Geometry and processes of electron-beam evaporation.

⊗ denotes **B** field pointing into the paper [58].

[1, 58]. The filament is at a high negative potential so those electrons are accelerated on to the source, which is at earth potential. To avoid dissolving the filament in arriving evaporant, the filament is located out of sight of the evaporant, and the electron-beam is pulled around and focused to the target surface by a magnetic field. The target surface will be heated at the site of the electron-beam incidence to the temperature required for evaporation. The evaporated particles will then travel in a vacuum (with a typical pressure value of 10^{-5} torr) with their thermal velocities along a straight line until they reach the substrate surface, which is fixed horizontally above the target material.

It is important to aim the beam at the center of the source material and to avoid hitting the material's container (the "hearth"). However, deposition uniformity is improved by scanning the beam around on the surface in a raster pattern. Without rastering, the evaporating material tends to be angularly distributed in a lobe-shaped pattern. The lobe is apparently due to collimation arising from the depression created in the surface by rapid evaporation from the point of beam impact. The source material is, usually, contained in a Cu "hearth" which is water-cooled to prevent its outgasing or alloying with molten source materials.

All evaporation done with narrow intense energy beams is subject to the "macro-particle spitting" problem [58]. The mechanism of macro-particle ejection is the sudden evaporation of a nodule of a particular contaminant whose vapour pressure is much higher than that of the source material. This sudden pressure burst can knock out from the surface a macro-particle of solid or liquid material typically 0.1 to 1 μm in diameter. The particle is likely to land on the depositing film. The macro-particle problem can be minimized using very pure source material.

Although electron-beam evaporation is a thermal process, the vapour atoms leave the surface with only thermal energy ~ 0.2 eV [58], several kinds of non-thermal energy still arrive at the film surface. One is x-ray generated by electron-beam impact on the source material. These x-rays are not energetic enough to be a hazard for the operator but they can be a hazard to the product. In particular, dielectric materials for electronic applications can develop undesired charge-trapping defects or embedded charge from x-ray irradiation. Another non-thermal energy accompanying electron-beam evaporation is the positive ions that are generated above the source by impact of the incoming beam upon the outgoing vapour as shown in Figure 1.1. By biasing the substrate negatively the ions can be accelerated into the depositing film. Because the resulting energy flux can be very large, it can have a profound effect on the film structure even though the fractional ionization of depositing vapour is small, a fact which applies to all of the deposition techniques that involve ions.

In some cases a gaseous species is introduced into the evaporation chamber for the purpose of forming a compound film by reaction with the evaporating species. The gaseous species will also become partially dissociated and ionized by collisions both with the electron beam and with the vapour ions if they are being accelerated toward the substrate. The ionized gas forms plasma between the source and the substrate. This gas activation assists the compound-film-formation reaction and is therefore a form of activated reactive evaporation.

The method enables us to attain a very high temperature condition and to evaporate materials, which would otherwise be evaporated with difficulty or can not be evaporated at all. An additional advantage of the method is the prevention of contamination by the evaporation source material; the beam heats only the evaporant whereas the support holder is usually cooled. At the same time no particles emitted

from the heated cathode- the source of the electron beam- can reach the substrate. Moreover another advantage of this method is that the source and the substrate can be conveniently heated to out-gas them.

1.3 Crystallographic properties of II-VI materials

The principal structure types for all II-VI compounds, with the exception of CdO, are cubic zincblende (sphalerite) and hexagonal wurtzite. The structures are based on the space groups F $\bar{4}$3m and P63mc. In the zincblende as well as in wurtzite structures, each atom of the metal (non-metal) is tetrahedrally surrounded by four atoms of the non-metal (metal) [1, 3].

In practice, crystals are usually nonideal and contain defects and imperfections, which in many cases control the semiconducting properties. Crystal imperfections are arbitrarily classified into point defects, such as vacancies or impurity atoms, line or plane defects, such as dislocations or stacking faults, and complex defects, which result from the interaction or coalescence of elementary defects [3, 64]. Description of zincblende and wurtize structures will be presented below.

1.3.1 Zincblende structure

Figure 1.2 shows the unit cell of the zincblende form of ZnS. There are four ZnS in a unit cell and all atoms occupy special positions with the coordinates: 4S in

$$000,0\frac{1}{2}\frac{1}{2},\frac{1}{2}0\frac{1}{2},\frac{1}{2}\frac{1}{2}0$$

and 4 Zn in

$$\frac{1}{4}\frac{1}{4}\frac{1}{4},\frac{1}{4}\frac{3}{4}\frac{3}{4},\frac{3}{4}\frac{1}{4}\frac{3}{4},\frac{3}{4}\frac{3}{4}\frac{1}{4}$$

Each Zn (S) atom has four nearest neighbours of S (Zn) at a distance of $((3/16)^{1/2}a_0)$ at the corners of a regular tetrahedron, where a_0 is the cubic lattice parameter. There are twelve next-nearest neighbours of atoms of the same kind at the distance $((2/4)^{1/2}a_0)$. Six of these are distributed at the corners of a hexagonal in the same plane as the original atom; the remaining six form a trigonal antiprism with three above and three below the plane of the hexagonal. An important aspect of the zicblende arrangement is the absence of a center of symmetry or inversion. The Zn-S layers have unique orientations along the <111> directions. As a result, zincblende crystals are polar and opposed (*h k l*) and ($\bar{h}\ \bar{k}\ \bar{l}$) faces and opposed [*h k l*] and [$\bar{h}\ \bar{k}\ \bar{l}$] directions may have different physical and chemical properties. A consequence is that zincblende crystals are piezoelectric. The Zn and S ions of opposite polarity are visualized as forming a network of permanent dipole moments. A mechanical distortion upsets the neutral balance of their moments and creates potential differences of opposite charge or tension and compression [3].

1.3.2 Wurtzite structure

There are two molecules in the hexagonal unit cell with two metal atoms at

$$000, \frac{1}{3}\frac{2}{3}\frac{1}{2}$$

And two non-metal atoms at

$$00u, \frac{1}{3}\frac{2}{3}\frac{1}{2}+u$$

With $u \approx 3/8$. Figure 1.3 shows the hexagonal form of ZnS. Each Zn atom is bonded to four S atoms, approximately at the corners of a tetrahedron, one at the distance

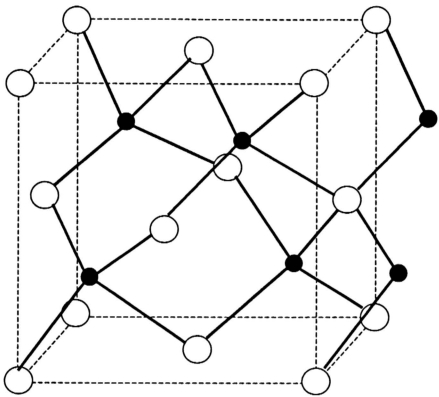

Figure 1.2: Zincblende. The arrangement of metal atoms (small filled circles) and non-metal atoms (large open circles) in zincblende, the cubic form of ZnS [3].

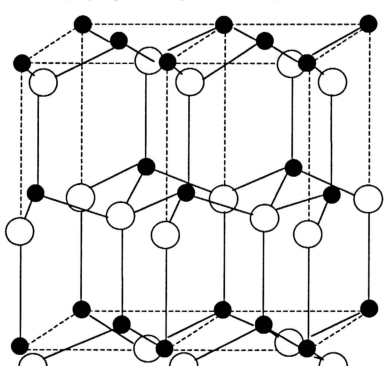

Figure 1.3: Wurtzite. The arrangement of metal atoms (small filled circles) and non-metal atoms (large open circles) in wurtzite, the hexagonal from of ZnS. The dashed lines outline the orthohexagonal cell for which $a_0 = (3)^{1/2} a_{0(hex)}$, $b_0 = a_{0(hex)}$, $c_0 = c_{0(hex)}$ and the cell edges are all at right angles to each other [3].

(uc_0) and three at $[1/3a_0^2 + c_0^2 (u - 0.5)^2]^{1/2}$. If ($c_0/a_0$) = 1.633, and if u = 0.375, the nearest-neighbour coordination figure is precisely tetrahdral and twelve next-nearest neighbour distances are equal. There is a close empirical correlation between c_0/a_0 and the stability of wurtzite or zincblende structures. The range of c_0/a_0 values for which the materials are dimorphous (both wurtzite and zincblende occur) extends equally about both sides of the ideal value (c_0/a_0=1.633). This suggests that the relationship between energy difference (stability) and $\Delta(c_0/a_0)$ is almost linear. The distortion (c_0/a_0) is strongly related to long-range coulomb effects, the covalent contribution being essentially independent of the material. Some correlation between (c_0/a_0) and the square of an effective charge parameter is therefore expected [1].

Wurtzite does not have a center of symmetry and there is a polar axis parallel to [0001]. As in zincblende, the II and VI ions of opposite polarity can be visualized as forming a network of permanent dipole moments. However, in wurtzite the moments do not balance but create a single polar axis. Consequently, in addition to being piezoelectric, wurtzite crystals are pyroelectric and may develop potential differences of opposite signs on heating and cooling [3].

1.3.3 Zinc sulphide (ZnS)

Both zincblende and wurtzite modifications of ZnS are found in natural deposits of ZnS. Wurtzite is the stable form at high temperature and inversion temperatures of 1020 ^{0} C and 1150 ^{0} C have been reported for the hexagonal to cubic transition [3]. There is considerable scatter in the values reported for the lattice constants of both cubic and hexagonal modifications and the variations appear to be due both to impurities and imperfections in the crystal structure [3]. However, Table 1.1 reports x-ray diffraction data for cubic and hexagonal ZnS systems [65].

1.3.4 Zinc selenide (ZnSe)

Zinc selenide usually crystallizes in the zincblende arrangements. The faulted or mixed crystals that may be obtained at 1050-1080 ^{0} C can be transformed to cubic by annealing at 900 ^{0} C [3]. The wurtzite modification has been prepared but there are conflicting values reported for the hexagonal cell constants [3]. The reported data of x-ray diffraction for cubic zinc selenide are shown in Table 1.2 [65].

1.3.5 Zinc sulpho-selenide (ZnS-ZnSe)

Crystals grown from combinations of II-VI compounds may be substitutional solid solutions or a mixture of zincblende and wurtzite modifications. The crystallographic nature of the mixture depends on the preparation conditions and the presence of impurities or additives. Substitutional solid solutions with the zincblende structure, which approximately obey Vegard's law over the complete range of composition, have been reported for ZnS-ZnSe [42, 48-50, 53]. Crystalline quality of ZnS_xSe_{1-x} epitaxial films grown on GaAs has been investigated [50]. The results have shown that the crystalline quality is affected by the fluctuation in orientation caused by lattice mismatch and partly by the fluctuation in spacing, which may be associated with an inhomogeneous distribution of S and Se atoms.

1.4 Band structure and optical properties

This section deals with the band structure of ZnS and ZnSe materials and important optical properties, which can be conceptually derived from it.

1.4.1 Band structure

Figure 1.4 shows the Brillouin zones in the reciprocal lattices of cubic zincblende and hexagonal wurtzite structures. Due to the similarity of crystal structure (both have four nearest neighbours for each atom and twelve next-nearest neighbours) there is a close correspondence between many parts of the two Brillouin zones.

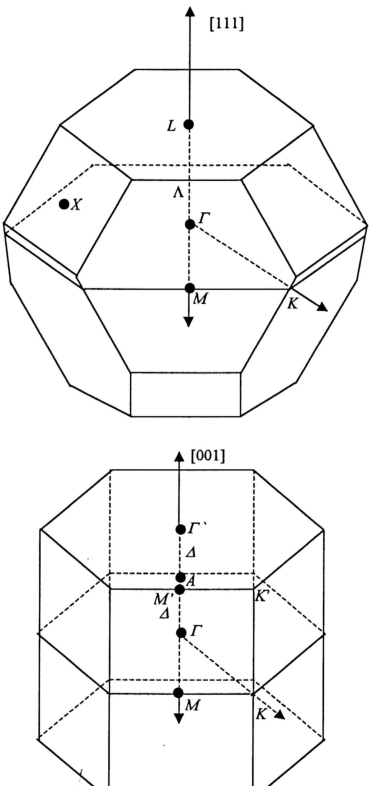

Figure 1.4: (a) Brillouin zone of the zincblende lattice and **(b)** double Brillouin zone of the wurtzite lattice [1].

Figure 1.5 shows schematically the band structure of II-VI compounds around Γ (reciprocal lattice vector $\mathbf{K} = 0$). As it follows from group theory [1] using the experimental information that all these materials are direct energy band gaps in the sense that the minimum of the conduction band and the maximum of the valence band are at $\mathbf{K} = 0$ and taking into account spin-orbit (s-o) coupling.

In the cubic symmetry T_d (Figure 1.5 (a)) there are a twofold degenerate conduction band (Γ_6) and the valence band (6 fold) is split by s-o coupling into a (higher) fourfold degenerate Γ_8 and a twofold Γ_7 (lower) valence band. Away from $\mathbf{K} = 0$ the Γ_8 splits into a light and a heavy hole band as shown in Figure 1.5 (a).

In the uniaxial wurtzite compounds (C6v) there are a twofold degenerate conduction band Γ_7 and more complex valence bands. Here the uniaxial crystal field splits the uppermost valence band into twofold bands Γ_9 and Γ_7 (if s-o coupling is positive). The detailed band structures of these compounds can be understood qualitatively from the fact that they are rather ionic and so the parts of their Bloch functions, which have the periodicity of the lattice, will be related to the parent atomic orbitals. The conduction band will be formed from the first unoccupied levels of the cations, i. e. the 4s or 5s levels of Zn and Cd, respectively. The uppermost valence bands will correspondingly be made up from the highest occupied levels of the anions namely the 2p, 3p and 4p levels of O, S and Se, respectively, the deeper lying d-levels might however admix into the valence bands. From this situation it follows that transitions between these bands will be dipole allowed. Detailed band structures of ZnS and ZnSe have been calculated using the pseudopotential method [66-68]. Figure 1.6 shows the band structure of ZnSe as calculated by Chelikowsky and Cohen [69]. Figures 1.7 (a) and (b) show the band structures of cubic and hexagonal ZnS respectively [68]. These calculations [68] neglect s-o coupling. Therefore, there is no

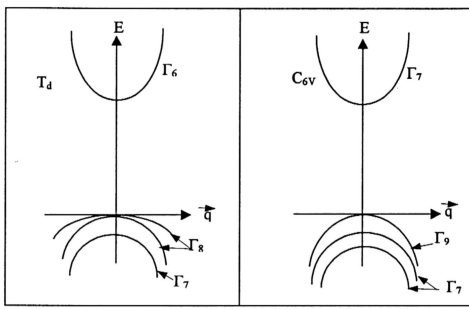

(a) **(b)**

Figure 1.5: A schematic drawing of the band structures at the Γ-point for **(a)** zincblende (T_d-symmetry) and **(b)** wurtzite (C_{6V}-symmetry) [1].

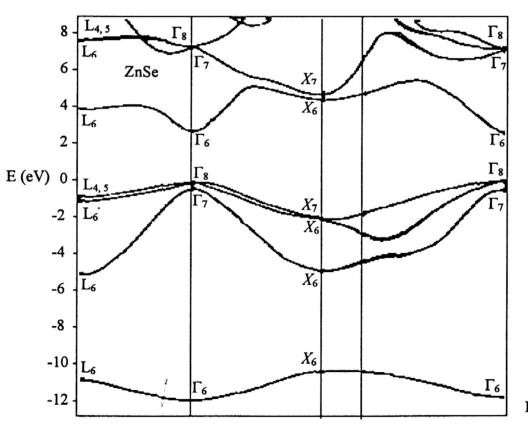

Figure 1.6: Band structure of ZnSe calculated by non-local pseudo-potential method [69].

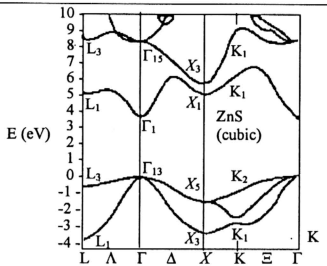

(a)

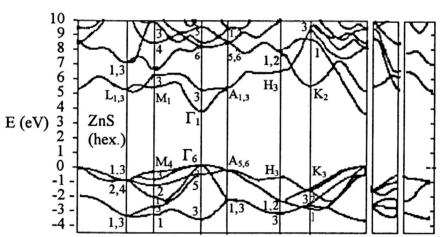

(b)

Figure 1.7: Band structure of cubic ZnS **(a)** and hexagonal ZnS **(b)** calculated using local pseudo-potential method [69].

s-o splitting of the valence bands as shown in Figure 1.7, the degeneracy of the Γ_{15}-valence band maximum will be split into Γ_8 and Γ_7 bands as shown in Figure 1.5. The general correspondence are T_d - Γ_{15} (no spin)$\rightarrow\Gamma_8 + \Gamma_7$(s-o) and Γ_1(no spin) $\rightarrow\Gamma_6$(s-o); C6v - Γ_1(no spin) $\rightarrow\Gamma_7$(s-o) and Γ_3(no spin) $\rightarrow\Gamma_7 + \Gamma_9$(s-o).

Due to the similarity of crystal structure of zincblende and wurtzite systems their band structures are not very different. The experiments to which band structure data should compare are optical absorption or reflectivity. The usual quantity calculated in connection with band structure calculations is the imaginary part of the dielectric function, which is related to the experimental values of refractive index and extinction coefficient [1]. In the absorption process, a photon of a known energy excites an electron from a lower to a higher energy state. So by exposing a semiconductor material to a light of different wavelengths from a monochromator and studying the changes in the transmitted radiation, one can analyze all possible transitions an electron can make and learn much about the distribution of states. These possible transitions are: band to band, excitons, between sub-bands, between impurities and bands, transitions by free carriers within a band, and also the resonance due to vibrational states of the lattice and of the impurities. In the following sub-section, the band to band transition related to this work will be described. The other transitions are described in references [1,3, 70].

1.4.2 Fundamental absorption

The fundamental absorption refers to the excitation of an electron from the valence band to the conduction band. The fundamental absorption which manifests itself by a rapid rise in absorption, can be used to determine the optical energy gap of the semiconductor. However, because the transitions are subject to certain selection rules, the estimation of the energy gap from the absorption edge is not a straight

forward. The rule governing the electron transitions from the valence band to the conduction band is the conservation of quasimomentum of the electron during the transitions. If the extrema of the valence and conduction bands lie at the same point of the **K**-space, the transitions are called direct. If this is not the case, the transitions are possible only when phonon-assisted and are called indirect. Typically for all direct semiconductors (if only intrinsic effects are taken into consideration) the absorption coefficient increases sharply from 1 to 10^5 cm^{-1} within a very small region of photon energies. This steepness of the absorption edge is characteristic of direct gap materials and stems from the fact that the lowest energy transition just at the edge is dipole allowed [1]. At low temperature a structure appears in the proximity of the absorption edge due to exciton absorption. The exciton can be presented by considering the basic electronic excitation in a perfect semiconductor at low temperature. This is the transfer of an electron from a filled valence band to an excited state leaving behind a hole with which the electron interacts via a coulomb interaction. This two-particle system, the interacting electron and hole together with the remainder of the crystal, constitutes the exciton system [3]. In some favourable cases at low temperatures the exciton structure can be used to define the energy gap. However, at higher temperatures or if the exciton spectrum can not be resolved (because of poor crystal quality) the fundamental energy gap has often been determined as the high-energy limit of transparency. In some measurements an exponential variation of the absorption coefficient with photon energy has been observed resulting in a so-called "Urbach edge". Urbach behaviour of the absorption edges of various semiconductors including the II-VI compounds was expected to be a result of the effects of the thermal expansion of the lattice and phonon interaction [1]. Because of their strong coupling to electrons and their high energy, the longitudinal optical (LO) phonons are

likely to make the largest contribution to the shift and the broadening of the absorption edge at least at temperatures where they are not completely frozen out.

In the visible region, near the fundamental edge the refractive index is highly dispersive. This dispersion of the refractive index is Kramers-Kronig related to the neighbouring absorption edge. The sharp rise of the refractive index near the absorption edge might profitably be used in optoelectronic designs.

Impurities, especially shallow coulomb centers in doped semiconductors, give rise to extrinsic absorption just below the gap. A so-called impurity tail at absorption coefficient below 10^2 cm^{-1} is quite common even for good crystals.

The dependence of the energy gap on the composition for mixed crystals formed from II-VI compounds, such as ZnS_xSe_{1-x}, has been investigated [41-44, 46-57]. In general, the energy gap obeys a quadratic behaviour with the composition. This behaviour is empirically described by a bowing parameter [1]. There is a large scatter in the bowing parameter values reported in the literature. For example, values in a range of 0 to 0.65 have been determined [1] for the bowing parameter for ZnS_xSe_{1-x} materials. This scatter in the values is due to the difficulty in the experimental determination of the energy gap in mixed crystals. As a rule the excitonic features in absorption or reflection are used in order to determine the dependence of the energy gap on the composition. Hence the binding energy of the exciton is assumed to depend linearly upon composition and the exciton line width broadening due to rather large disorder effects in II-VI mixed crystals is neglected. The disorder induced broadening of line width can be of the order of 10 meV.

1.5 Electrical properties

The electrical properties of a semiconductor are mostly characterized by the conductivity σ (or its reciprocal value, the resistivity ρ), the concentration of the free

carriers, and carrier mobility. These three quantities can be deduced from the measured values of the conductivity and Hall effect measurements.

Like the optical properties, the electrical quantities depend ultimately on the electronic band structure, which determines the intrinsic carrier concentration, and on the lattice vibrational modes, which set upper limits on the electron and hole mobilities. In II-VI compounds, the strongest influence on the electrical properties comes from impurities and native defects, which are introduced into the materials during their preparation either deliberately or unintentionally. These impurities and defects act as sources of free carriers and as scattering centers that reduce the mobility to values greatly below the lattice scattering limit. However, in the wide gap materials, the intrinsic carriers do not make a significant contribution to the conductivity, and the free carriers for low-resistivity conduction have to be produced by the incorporation of donor and acceptor into the material. In principle, extrinsic carrier concentrations can be generated by the ionization of impurities, native defects, or complexes among them.

The observed activity of the substitutional impurity can be explained by the rule that it is a donor or acceptor depending on whether it has more or less valence electrons than the atom it replaces. Native point defects (vacancies and interstitials, that cause deviations from the stoichiometric composition of the compound) associated with excess metal (non-metal vacancies and metal interstitials) are believed to be mostly donors and defects associated with excess non-metal (metal vacancies and non-metal interstitials) are believed to be acceptors [1].

As for complexes, the most important centers appear to be simple pairs of impurities and native defects. For instance, the formation of an acceptor by pairing of donor impurities with zinc vacancies has been discussed as the primary cause of

composition effects in high-purity n-type ZnS and ZnSe [1, 3]. A quantitative treatment of the extrinsic carrier concentration and carrier mobility for II-VI materials has been intensively presented [1, 3]. In the following, the temperature-dependence of the dc-conductivity and the electronic conduction mechanisms will be discussed. But before that, the theoretical models and concepts, which have been proposed for describing the electronic states to understand the conduction mechanisms in materials, will be presented.

1.5.1 Energy band models

The purpose of the energy band models is to provide an understanding of the density of extended and localized states and the mobility of the charge carriers and hence the conduction mechanism through the material can be understood. The density of electronic states is an applicable concept to both crystalline and non-crystalline materials, implying the applicability of band models to any material. The density of states is denoted by $N(E)$ and is defined so that $N(E)\,dE$ is the number of eigenstates in unit volume for an electron in the system with given spin direction and with energy between E and $E + dE$.

Mott-CFO model

This model is sketched in Figure 1.8 and is derived from the concept of an ideal covalent random network structure. Simple chemical considerations as well as the observation that amorphous semiconductors are transparent in the infrared and exhibit a thermally activated conductivity suggest that the valence and conduction bands are separated by a gap. Translational and compositional disorder are assumed to cause fluctuations of the potential of sufficient magnitude that they give rise to localized states extending from the conduction and valence bands into the gap [71]. These localized states are not associated with definite imperfections but are the result

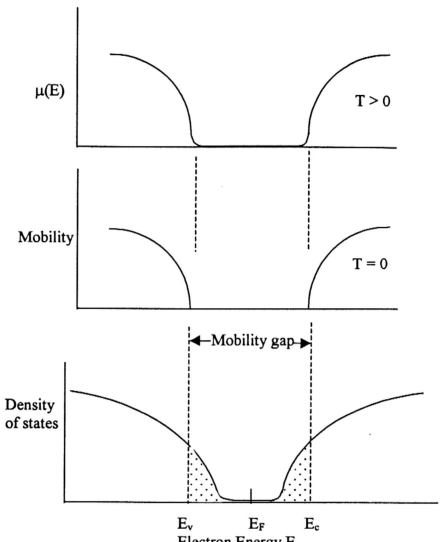

Figure 1.8: Sketch of Mott-CFO model for covalent semiconductors having three-dimensional cross-linked network structure. The critical energies E_c and E_V define the mobility gap. For $T > 0$ the mobility $\mu(E)$ may be finite in the gap because of thermally assisted tunneling. E_F is the Fermi energy. The distribution of localized gap states may be non-monotonic when defect states of a certain energy are prevalent [71].

of the randomness of the potential. Their number and energy spread increases with the degree of randomness and the strength of the scattering. The valence band tail states are assumed to be neutral when occupied and the conduction band tail states are neutral when empty [71]. This assumption places the Fermi energy level somewhere near the gap center. In addition the deviations from the ideal covalent random network, such as vacancies, dangling bonds, and chain ends, are expected to contribute to localized states in certain energy ranges. These then give rise to a non-monotonic density of localized states curve. It is noted [72] that the character of the wave functions changes at critical energies E_c and E_v, which separate the extended and the localized states. Here the electron and hole mobilities drop sharply from a low-mobility band transport with finite mobility at zero temperature to a thermally activated tunneling between localized gap states which disappears at zero temperature. These so-called mobility edges define a mobility gap, E_c-E_v, which contains only localized states. This model is believed to be applicable to alloy glasses, which contain compositional as well as positional disorder.

Davis-Mott model

This model is sketched in Figure 1.9. The mobility edges for electrons and holes lie at E_c and E_v. In this model distinction is made between localized states which originate from lack of long-range order and others which are due to defects in the structure. The first kind of localized states extended only to E_A and E_B in the mobility gap. The defects states form longer tails but of insufficient density to pin the Fermi level. Moreover, a band of compensated levels near the gap center is proposed [72] in order to pin the Fermi level and to account for the behaviour of the ac-conductivity.

Marshall-Owen model

This model is shown in Figure 1.10. The position of the Fermi level is determined by bands of donors and acceptors in the upper and lower halves of the mobility gap, respectively. The concentrations of donors and acceptors adjust themselves by self-compensation to be nearly equal so that the Fermi level remains near the gap center. At low temperature it moves to one of the impurity bands because self-compensation is not likely to be complete [71].

Sharph band edge model

Molecular solids and tight binding, semi-insulating materials with large gaps have electronic structures, which are relatively insensitive to disorder [71]. In these materials, tail states are negligible and a band model not significantly different from that of crystals with sharp band edges is appropriate. Since the molecular units are well-defined entities it is expected [71] that the energies of localized defect states fall into rather narrow energy ranges deep in the gap. Because the energy to create a defect state is of the order of the band gap, their number will be small and self-compensation as well as association of donor and acceptor type defects are energetically favoured.

1.5.2 Temperature dependence of dc-conductivity

With the model proposed by Mott and Davis [72] for the density of states and mobilities in an amorphous semiconductor, three mechanisms of electrical conduction can be distinguished:

(a) Conduction due electrons excited above E_c or E_v into non-localized or extended states. If the main current is carried by electron the conductivity σ is given [71] by

$$\sigma = \sigma_0 \exp\left[-(E_c - E_F)/K_\beta T\right] \quad \text{.....(1.1)}$$

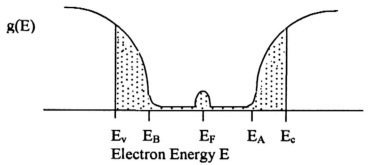

Figure 1.9: Density of states g(E) suggested by Davis and Mott [79]. E_c-E_V is the mobility gap. The ranges E_c-E_A and E_B-E_V contain localized states originating from lack of long-range order. Thermally assisted hopping may take place in these ranges. A band of compensated levels is proposed to lie near the gap center [71].

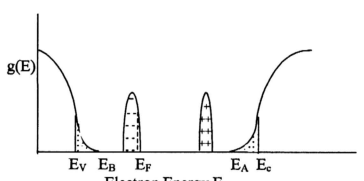

Figure 1.10: Density of states g(E) suggested by Marshal and Owen for As_2Se_3. The energies E_V, E_B, E_A, and E_c have the same meaning as in Figure 1.9. A band of localized acceptor states lies below and a band of donor states above the gap center. In the cases shown, the acceptors are nearly compensated by the donors. As T is increased E_F moves toward the gap center [71].

where K_β is Boltzmann constant and T is the absolute temperature. The pre-exponential factor σ_0 is given by

$$\sigma_0 = eN(E_c)K_\beta T\,\mu_0 \quad \text{.....(1.2)}$$

where e is the electronic charge and μ_0 is the mobility in extended states. Since σ_0 is expected to be temperature independent then μ_0 is proportional to $1/T$. The separation of E_F from the mobility edge will change with T. assuming in the temperature range of interest linear temperature dependence as

$$E_c - E_F = \Delta E_1 - \gamma T \quad \text{.....(1.3)}$$

where γ is a constant and ΔE_1 is the activation energy required for electron to jump between neighbouring sites. A plot of ln (σ) against $1/T$ will yield a straight line with a slope of $\Delta E_1/K_\beta$ and an intercept on the σ axis of $\sigma_0 \exp(\gamma/K_\beta)$. In the case of ambipolar conduction, the exponential term describing the conduction of holes has to be added to equation 1.1. Depending on the relative magnitudes of the prefactors and the activation energies, it is then possible that the conductivity curve has two slopes with one type of carrier dominating at low T and the other at high T. The conductivity does not follow a simple exponential law when ΔE_1 depends on T as a result of a temperature dependent shift of E_F. Such a shift results from the neutrality condition when $N(E)$ is symmetric with respect to E_F.

(b) Thermally assisted tunneling into the localized states at the band edges i. e. at E_A and E_B in Figure 1.9 or into the donor or acceptor bands of Figure 1.10. The largest tunnel contribution arises from jumps to unoccupied levels of nearest neighbour

centers. Since it is unlikely to find such a level at the same energy, the tunneling process is usually inelastic i.e. it involves the emission or absorption of a phonon. Hence this thermally assisted tunneling process involves a hopping energy ΔW_1 in addition to the activation energy E-E_F needed to raise the electron to the appropriate localized state at E. If the main current is carried by electrons, and conduction is by hopping, then

$$\sigma = \sigma_1 \exp\left[-\left(E_A - E_F + \Delta W_1\right)/K_\beta T\right] \quad \text{.....(1.4)}$$

σ_1 is expected to be a factor of 10^2-10^4 less than σ_0, due partly to an effective density of states lower by a factor ~ $(E_c$-$E_A)/\ K_\beta T$, but mainly to a lower mobility. The conductivity curve is not expected to exhibit constant activation energy unless the mobility does not fall off too rapidly between E_c and E_A.

(c) Conduction due to carriers hopping (tunneling) between localized states near the Fermi energy level. This process is analogous to impurity-conduction in heavily doped semiconductors. The conductivity is given [72] by

$$\sigma = \sigma_2 \exp\left[-\Delta W_2/K_\beta T\right] \quad \text{.....(1.5)}$$

where $\sigma_2 << \sigma_1$ and ΔW_2 is the hopping energy. It is emphasized that a straight line in a plot of lnσ against $1/T$ is expected if hopping is between nearest neighbours. As the temperature is lowered, the number and energy of phonons available for absorption decreased so that tunneling is restricted to seek centers which are not nearest neighbours but which instead lie energetically closer and with the range $K_\beta T$. Ultimately the so-called variable range hopping process [72] takes place. In this process the conductivity is expected to vary as $(1/T)^{1/4}$.